Computational Materials Science 50 (2010) 32–42

Contents lists available at ScienceDirect

Computational Materials Science

journal homepage: www.elsevier.com/locate/commatsci

Modelling mixed columnar-equiaxed solidification with melt convection and grain sedimentation – Part I: Model description

M. Wu *, A. Fjeld, A. Ludwig

Chair for Simulation and Modelling of Metallurgical Processes, Department of Metallurgy, University of Leoben, A-8700 Leoben, Austria

ARTICLE INFO

Article history:
Received 8 June 2010
Accepted 8 July 2010
Available online 4 August 2010

Keywords:
Solidification
Equiaxed
Columnar
Dendrite
Convection
Sedimentation

ABSTRACT

Part I of this two-part investigation presents a volume-averaging multiphase solidification model that accounts for mixed columnar-equiaxed solidification, non-dendritic and dendritic crystal growth, nucleation of equiaxed grains, columnar primary dendrite tip tracking, melt flow, sedimentation of equiaxed crystals, and their influence on macrostructure and macrosegregation. Five distinct thermodynamic phases (phase regions) are defined: solid dendrites in equiaxed grains, the interdendritic melt between equiaxed dendrites, solid dendrites in columnar trunks, the interdendritic melt between trunk dendrites, and the extradendritic melt. These five phase regions are quantified by their volume fractions and characterized by their solute concentrations. The five phase regions are grouped into three hydrodynamic phases: equiaxed grains consisting of solid dendrites and interdendritic melt, columnar trunks consisting of solid dendrites and interdendritic melt, and extradendritic melt. The extradendritic melt is separated from the interdendritic melt with a grain envelope, whose profile connects the primary, secondary or tertiary dendrite tips to form a 'natural' enclosure of the equiaxed grains or columnar trunks. The envelope is further simplified as a volume-equivalent sphere for equiaxed grains, or as volume-equivalent cylinder for columnar trunks by use of morphological shape factors. Expansion of the envelopes during solidification is determined by dendrite growth kinetics, using the Kurz–Giovanola–Trivedi model for growth of columnar primary dendrite tips and the Lipton–Glicksman–Kurz model for growth of columnar secondary dendrite tips (radial growth of the columnar trunk) and equiaxed primary dendrite tips. The solidification of the interdendritic melt is driven by the supersaturation of the interdendritic melt and governed by the diffusion in the interdendritic melt region. Illustrative process simulations and model verifications are presented in Part II.

1. Introduction

Although significant progress has been made in the last century with respect to understanding mixed columnar-equiaxed solidification, accurately modelling such solidification at the process scale remains a significant challenge. Demand in industry for such a model is high with the assumption that the ability to control and dictate as-cast macrostructure would be improved. The complex interactions of multiphase flow, multiple grain morphologies, and multiscale phenomena contribute to the following four points that a successful model with predictive capabilities must address:

(1) Solidification phenomenon spans a wide range of length scales with global transport phenomena occurring at the process scale (∼m) and crystal growth kinetics, governed mainly by the chemical diffusion, occurring at the microscopic scale (∼μm).
(2) Different grain morphologies must be properly incorporated into the macro model. An equiaxed grain may initially grow with a globular morphology followed by dendritic morphology while a columnar trunk may grow with cellular or dendritic morphology. The transition between non-dendritic and dendritic growth has significant impact on the microstructure evolution.
(3) For the solidification of most metal alloys both columnar and equiaxed structures (morphologies) co-exist. Competition between them often occurs during solidification process, causing the columnar-to-equiaxed transition (CET).
(4) The solidification process is always accompanied with multiphase transport phenomena of the bulk and interdendritic flow, flotation and sedimentation of free crystals.

In the previous decades numerous models have been proposed to address the above difficulties. Wang and Beckermann are the leading authors among those who have used a multiphase, volume-averaged approach to bridge the length scales between global transport phenomena and microscopic crystal growth kinetics

* Corresponding author.
E-mail address: menghuai.wu@mu-leoben.at (M. Wu).

0927-0256/$ - see front matter © 2010 Elsevier B.V. All rights reserved.
doi:10.1016/j.commatsci.2010.07.005

Nomenclature

c_ℓ, c_e, c_c concentration of hydrodynamic ℓ-, e-, or c-phase (wt.%)
$\bar{c}^c_{env}$ average concentration at columnar tree-trunk envelope (wt.%)
$\bar{c}^e_{env}$ average concentration at equiaxed grain envelope (wt.%)
c^c_d, c^c_s concentrations of interdendritic melt and solid dendrites in columnar tree trunk (wt.%)
c^e_d, c^e_s concentrations of interdendritic melt and solid dendrites in equiaxed dendritic grain (wt.%)
c^*_ℓ, c^*_s equilibrium concentration at liquid–solid interface (wt.%)
C_{ec} total species exchange between equiaxed grain and columnar trunk ($kg\cdot m^{-3}\cdot s^{-1}$)
$C_{\ell c}$ total species exchange between extradendritic liquid and columnar trunk ($kg\cdot m^{-3}\cdot s^{-1}$)
$C_{\ell e}$ total species exchange between extradendritic liquid and equiaxed grain ($kg\cdot m^{-3}\cdot s^{-1}$)
C^c_{ds} species transfer from d-phase to s-phase in columnar trunk ($kg\cdot m^{-3}\cdot s^{-1}$)
C^e_{ds} species transfer from d-phase to s-phase in equiaxed grain ($kg\cdot m^{-3}\cdot s^{-1}$)
$C^D_{\ell c}$ diffusive species exchange between extradendritic liquid and columnar trunk envelope ($kg\cdot m^{-3}\cdot s^{-1}$)
$C^M_{\ell c}$ species exchange at ℓ–e interface due to growth of columnar trunk envelope ($kg\cdot m^{-3}\cdot s^{-1}$)
$C^D_{\ell e}$ diffusive species exchange between extradendritic liquid and equiaxed grains ($kg\cdot m^{-3}\cdot s^{-1}$)
$C^M_{\ell e}$ species exchange at ℓ–e interface due to growth of equiaxed grain envelope ($kg\cdot m^{-3}\cdot s^{-1}$)
D_ℓ, D_s diffusion coefficient in liquid or solid phase ($m^2\cdot s^{-1}$)
d^c average diameter of columnar tree trunk (m)
d^e average diameter of equiaxed grain diameter (m)
d_2 diameter of second dendrite arm (m)
f_ℓ, f_e, f_c volume fraction of hydrodynamic ℓ-, e-, or c-phases (l)
f^c_s, f^c_d volume fraction of solid dendrites or interdendritic melt in columnar tree trunk (as fraction of total volume) (l)
f^e_s, f^e_d volume fraction of solid dendrites or interdendritic melt in equiaxed grain (as a fraction of total volume) (l)
f^{free}_c critical volume fraction of columnar phase for entrapment of equiaxed grains (l)
$f_{e,CET}$ hard blocking criterion (Hunt model) (l)
f^{extra}_{Eu} extradendritic eutectic phase (l)
$f^{intern}_{Eu,e}$, $f^{intern}_{Eu,c}$ interdendritic eutectic phases in equiaxed or columnar phase (l)
f^{total}_{Eu} total eutectic phase (l)
h_ℓ, h_e, h_c enthalpies of hydrodynamic ℓ-, e-, or c-phases ($J\cdot kg^{-1}$)
i_c status index for columnar tip tracking (l)
J^c_ℓ species diffusive flux from columnar trunk envelope into extradendritic melt ($m\cdot s^{-1}$)
J^e_ℓ species diffusive flux from equiaxed grain envelope into extradendritic melt ($m\cdot s^{-1}$)
k solute partitioning coefficient at the liquid–solid interface (l)
k_1 growth parameter in KGT model ($m\cdot s^{-1}\cdot K^{-2}$)
k_2 growth parameter in KGT model ($m\cdot s^{-1}\cdot K^{-3}$)
l length of the columnar trunk in the tip volume element (m)
l_{ref} reference length of volume element (columnar tip tracking) (m)
l^c_d, l^e_d diffusion length of interdendritic melt in columnar trunk or equiaxed grain (m)
l^c_ℓ diffusion length in extradendritic melt around columnar trunk envelope (m)
l^e_ℓ diffusion length in extradendritic melt around equiaxed grain envelope (m)
m_ℓ liquidus slope of binary phase diagram (K)
$M^c_{tip'}$ net mass transfer rate swept by the columnar primary dendrite tips ($kg\cdot m^{-3}\cdot s^{-1}$)
$M_{ce}(=-M_{ec})$ columnar-equiaxed net mass transfer rate ($kg\cdot m^{-3}\cdot s^{-1}$)
$M_{\ell e}(=-M_{e\ell})$ liquid-equiaxed net mass transfer rate ($kg\cdot m^{-3}\cdot s^{-1}$)
$M_{\ell c}(=-M_{c\ell})$ liquid-columnar net mass transfer rate ($kg\cdot m^{-3}\cdot s^{-1}$)
M^c_{ds} interdendritic solidification rate in columnar trunk ($kg\cdot m^{-3}\cdot s^{-1}$)
M^e_{ds} interdendritic solidification rate in equiaxed grain ($kg\cdot m^{-3}\cdot s^{-1}$)
n_e equiaxed grain number density (m^{-3})
n_c number density of columnar dendrites in the tip element (m^{-3})
p pressure shared by all phases ($N\cdot m^{-2}$)
R^c radius of columnar tree trunk (volume-equivalent cylinder) (m)
R^e radius of equiaxed grain (volume-equivalent sphere) (m)
R^c_f maximum radius of a columnar trunk envelope (m)
R^e_f maximum radius of an equiaxed grain envelope (m)
$R^c_{tip'}$ radius of columnar primary dendrite tip (m)
$S^c_{env,D}$ diffusion surface concentration of the columnar tree-trunk envelope considering dendritic morphology (m^{-1})
$S^c_{env,M}$ surface concentration of columnar tree trunk (volume-equivalent sphere for dendrite envelope) (m^{-1})
$S^e_{env,D}$ diffusion surface concentration of the equiaxed grain envelope considering dendritic morphology (m^{-1})
$S^e_{env,M}$ surface concentration of equiaxed grain (volume-equivalent sphere for dendrite envelope) (m^{-1})
S_{parab} surface area of paraboloid (columnar dendrite tip) (m^2)
S^c_s, S^e_s s–d interface concentration in columnar or equiaxed phase (m^{-1})
ΔS area of element size (2D mesh) (m^2)
Δt calculation time step (s)
T_ℓ, T_e, T_c temperatures of hydrodynamic ℓ-, e-, or c-phases (K)
T_E temperature of eutectic reaction (K)
ΔT undercooling (K)
$\vec{u}_\ell$, $\vec{u}_e$, $\vec{u}_c$ velocity vector of hydrodynamic ℓ-, e- or c-phase ($m\cdot s^{-1}$)
v^c_{cell} growth velocity of cellular trunk ($m\cdot s^{-1}$)
v^c_{env} growth velocity of columnar trunk ($m\cdot s^{-1}$)
$v^c_{env,M}$ growth velocity of columnar trunk (volume-equivalent cylinder for dendrite envelope) ($m\cdot s^{-1}$)
$v^c_{tip'}$ growth velocity of columnar primary dendrite tip ($m\cdot s^{-1}$)
$v^c_{tip''}$ growth velocity of columnar secondary dendrite tip ($m\cdot s^{-1}$)
v^e_{glob} growth velocity of equiaxed grain (globular) ($m\cdot s^{-1}$)
v^e_{env} growth velocity of equiaxed grain ($m\cdot s^{-1}$)
$v^e_{env,M}$ growth velocity of equiaxed grain (volume-equivalent sphere for dendrite envelope) ($m\cdot s^{-1}$)
$v^e_{tip'}$ growth velocity of equiaxed dendrite tip ($m\cdot s^{-1}$)
v^e_{sd}, v^c_{sd} growth velocity of s–d interface in the equiaxed or columnar phase ($m\cdot s^{-1}$)
V_{parab} volume of paraboloid (columnar dendrite tip) (m^3)
ΔV volume of volume element (3D mesh) (m^3)
x, y, z coordinate (m)
α^c_d, α^c_s volume fraction of interdendritic melt or solid dendrites inside the columnar tree trunk ($\alpha^c_d + \alpha^c_s = 1$) (1)
α^e_d, α^e_s volume fraction of interdendritic melt or solid dendrites inside the equiaxed dendritic grain ($\alpha^e_d + \alpha^e_s = 1$) (1)
β_2 a constant ($\sim$1) in Eq. (17) (1)
Φ^c_{circ} circularity of the envelope of the columnar dendritic trunk (1)

Φ^{c}_{env}	shape factor of columnar dendrite trunk (1)
Φ^{c}_{Imp}	impingement factor for growth of columnar trunk (1)
Φ^{e}_{env}	shape factor of equiaxed dendritic grain (1)
Φ^{e}_{Imp}	impingement factor for equiaxed grain growth (1)
Φ^{e}_{sph}	sphericity of equiaxed grain envelope (1)
Φ^{s}_{Imp}	impingement factor for interdendritic melt solidification (1)
Γ	Gibbs–Thomson coefficient (m·K)
λ_1	primary dendrite arm space of columnar tree trunk (m)
λ_2	secondary dendrite arm space (m)
ρ^{c}_{d}, ρ^{e}_{d}	density of interdendritic melt in columnar trunk or equiaxed grain (kg·m^{-3})
ρ^{c}_{s}, ρ^{e}_{s}	density of solid dendrites in columnar or equiaxed phase (kg·m^{-3})
ρ_ℓ, ρ_e, ρ_c	average densities of hydrodynamic ℓ-, e-, or c-phases (kg·m^{-3})
Ω	supersaturation (l)

(points 1 and 4) [1–4]. In their work, the exchange and interaction phenomena between the solidifying structures and the liquid phase, which occur at the microscopic scale, are volume-averaged and incorporated into the macroscopic model for the transport phenomena occurring at the process scale. Rappaz and Thévoz proposed a micro–macro model or solute diffusion model to incorporate the dendritic crystal morphology into the global transport system (point 2) [5–7] and the interdendritic melt is treated as a separate phase (more precisely, phase region) from the extradendritic melt, separated by a fictitious grain boundary envelope. For the case of pure equiaxed solidification the globular-to-dendritic transition was subsequently included in this model by Appolaire and co-workers [8,9]. Some ideas to treat the columnar-to-equiaxed transition were proposed (point 3) [2,10–13], but the growth of the columnar dendrites were over-simplified in those previous models. The columnar primary dendrite tip front was not explicitly tracked. Great efforts were made to deal with the melt flow and transport of free crystals (point 4) [3,4,14–18], but no aforementioned model treats both columnar and equiaxed solidification simultaneously. The most sophisticated model dealing with mixed (3-phase) columnar-equiaxed solidification considering points 1, 3 and 4 was proposed by the current authors [19–21], where it was demonstrated that the 3-phase model can account for melt convection and grain sedimentation, macrosegregation, columnar-to-equiaxed-transition (CET), and macrostructure. The major drawback of the authors' 3-phase model is that the dendritic morphology is not addressed.

The current work extends the authors' previous 3-phase mixed columnar-equiaxed solidification model [19–21] by incorporating the dendritic morphologies. Based on the original models of Rappaz and Thévoz [5,6] and Wang and Beckermann [2,4], the authors have proposed a modified equiaxed solidification model to treat the dendritic morphology [22,23]. Improvements in the authors model include the globular-to-dendritic transition (GDT); the non-uniform solute distribution in the interdendritic melt region during dendritic growth; the diffusion-governed solidification of the interdendritic melt; and use of a hydrodynamic phase for equiaxed grains consisting of solid dendrites and interdendritic melt. In order to establish a mixed columnar-equiaxed solidification model considering these four aspects, a five-phase model is proposed. The current paper gives a detailed description of the model, including phase definitions, treatment of equiaxed and columnar dendrite morphologies and growth kinetics, and subsequent implementation in global transport equations. Illustrative process simulations and model verifications are made in Part II.

2. Phase definition

As schematically shown in Fig. 1, two types of crystal morphologies co-exist in conventional solidification processes: equiaxed and columnar. Immediately following the formation of fine equiaxed crystals near the casting surface (chill zone), columnar dendrites begin to grow from the mould surface towards the hot casting centre while freely moving equiaxed grains continue to nucleate in the vicinity of the primary dendrite tips and in the bulk melt region. To describe the hydrodynamic behaviour of the equiaxed grains, the columnar trunks and surrounding melt, three hydrodynamic phases are defined respectively as e-, c- and ℓ-phases. They are quantified with their volume fractions f_e, f_c, f_ℓ and they move with corresponding velocity $\vec{u}_e, \vec{u}_c$, and $\vec{u}_\ell$. The velocity of the c-phase, $\vec{u}_c$, is predefined (zero in this case).

If the equiaxed grains and columnar trunks are dendritic, two distinct phase regions exist within an equiaxed grain or a columnar trunk: the solid dendrites and interdendritic melt. It is assumed that the interdendritic melt is transported with the solid dendrites and is generally more enriched with solute element than the extradendritic melt surrounding the grains. In this sense, a fictitious grain boundary envelope must be constructed to separate the interdendritic melt from the extradendritic melt. Therefore, during the mixed columnar-equiaxed solidification five thermodynamic phase regions can be defined: the solid dendrites in the equiaxed grain, the interdendritic melt in the equiaxed grain, the solid dendrites in the columnar dendrite trunk, the interdendritic melt in the columnar dendrite trunk, and the extradendritic melt. They are quantified with volume fractions (f^e_s, f^e_d, f^c_s, f^c_d, f_ℓ), and characterized by their corresponding solute concentrations (c^e_s, c^e_d, c^c_s, c^c_d, c_ℓ).

The two thermodynamic phases of an equiaxed grain, the solid dendrites and interdendritic melt, combine to form a single hydrodynamic phase, e-phase, moving with the velocity $\vec{u}_e$, similarly, the thermodynamic phases in a columnar trunk, the solid dendrites and interdendritic melt, form a second hydrodynamic phase, c-phase, moving with a predefined velocity $\vec{u}_c$. The remaining thermodynamic phase, the extradendritic melt, ℓ-phase, singly forms the third hydrodynamic phase. The volume fraction of each phase region inside the grain envelope is denoted as $\alpha^e_d, \alpha^e_s, \alpha^c_d, \alpha^c_s$ with subscripts d for interdendritic liquid and s for dendritic solid. For example, inside an equiaxed grain, volume fractions of interdendritic liquid and dendritic solid are quantified respectively with α^e_d, α^e_s, hence $f^e_d = \alpha^e_d \cdot f_e$ and $f^e_s = \alpha^e_s \cdot f_e$. For a globular equiaxed grain, $\alpha^e_d = 0$, hence $f^e_s = f_e$. Inside a columnar dendrite trunk, volume fractions of two-phase regions are quantified with α^c_d, α^c_s, hence $f^c_d = \alpha^c_d \cdot f_c$ and $f^c_s = \alpha^c_s \cdot f_c$. For a cellular trunk, $\alpha^c_d = 0$, hence $f^c_s = f_c$.

The velocity and temperature fields are solved for all hydrodynamic phases. The transport of mass and species of each thermodynamic phase is calculated according to the velocity of the corresponding hydrodynamic phase. As shown in Fig. 1, the columnar primary dendrite tip front is explicitly tracked. The columnar primary dendrite tip front divides the calculation domain into two. In front of the columnar dendrite tip front, the maximum number of hydrodynamic phases is two, i.e. ℓ-phase and e-phase, and the maximum number of thermodynamic phases is three.

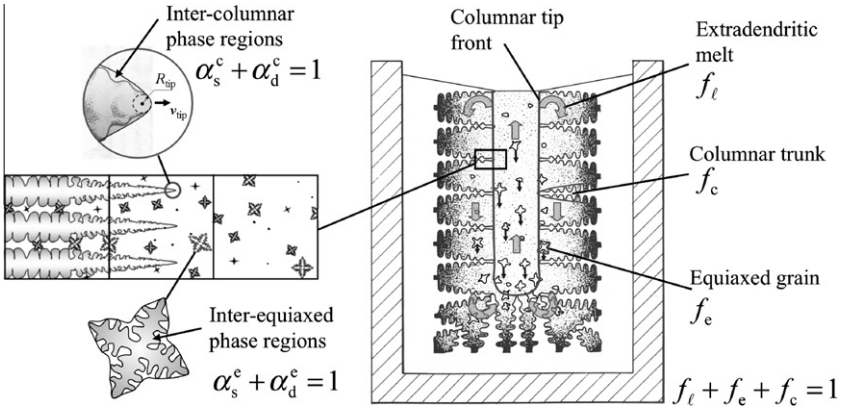

Fig. 1. Schematic of the mixed columnar-equiaxed solidification.

However, behind the columnar dendrite tip front, all three hydrodynamic phases and all five thermodynamic phases are involved.

3. Growth kinetics

3.1. Equiaxed growth

3.1.1. Equiaxed grain morphology

Immediately after nucleation an equiaxed grain begins to grow with globular morphology, which can be simplified as sphere. The growth of a spherical grain was described in detail in a previous publication [17,18]. Following the globular-to-dendritic transition [22], the grain growth becomes dendritic. As shown in Fig. 2, the grain envelope (dashed line) of the equiaxed grain is defined as a fictitious surface contour connecting the primary and secondary dendrite tips. The interdendritic melt has an average concentration c_d^e, while the extradendritic melt has concentration c_ℓ. Species exchange between the inter- and extradendritic melts due to both grain growth and species diffusion across the grain envelope are computed. Continuity solute distribution across the grain envelope must be satisfied and the average concentration at the grain envelope $\bar{c}_{env}^e$ is neither equal to c_d^e nor to c_ℓ. Solidification occurs at the liquid–solid interface, i.e. the interface between the interdendritic melt and solid dendrites. The interdendritic melt and solid dendrites adjacent to the liquid–solid interface have thermodynamic equilibrium concentrations, c_ℓ^* and c_s^*; curvature effects are neglected. In the interdendritic melt, it is the concentration difference $(c_\ell^* - c_d^e)$ that serves as driving force for the solidification of the interdendritic melt. Solute partitioning $(k = c_s^*/c_\ell^*)$ occurs at the liquid–solid interface.

Due to the geometrically complex shape of the grain envelope (dashed line in Fig. 2) the growth rate of the grain cannot be easily quantified, however the primary dendrite tip growth velocity, $v_{tip'}^e$, according to, for example, Lipton–Glicksman–Kurz (LGK) model [24,25] can be determined. Therefore, the profile of the grain envelope is further simplified as a volume-equivalent sphere, with volume equal to that of the grain envelope. The correlation between the growth velocity of the equivalent sphere and the primary dendrite tip is made by introducing a shape factor $\Phi_{env,}^e$ [22,23] where

$$v_{env,M}^e = \Phi_{env}^e \cdot v_{tip'}^e. \tag{1}$$

In order to calculate the species diffusive flux across the grain envelope from the interdendritic melt to the extradendritic melt, however, the real surface area of the envelope $S_{env,D}^e$ is required. This area $S_{env,D}^e$ is correlated to the surface area of the equivalent sphere $(S_{env,M}^e)$ via a sphericity shape factor Φ_{sph}^e,

$$S_{env,D}^e = S_{env,M}^e / \Phi_{sph}^e. \tag{2}$$

Both Φ_{env}^e and Φ_{sph}^e are morphological shape factors, dependent purely on the shape of the grain envelope. If the shape of the envelope is known and preserved during solidification, both factors should be constant and can be predefined [5,6,8,9,26,27]. Examples of some equiaxed dendrites and their morphological shape factors are collected in Table 1. The accuracy and sensitivity of these shape factors will be addressed with model parameter studies. For solidification of globular grains both Φ_{env}^e and Φ_{sph}^e are equal to one.

Knowing the number density of the equiaxed grains n_e by solving the nucleation law and grain transport equation [17,18], the diameter of the volume-equivalent sphere d^e $(=2R^e)$ is calculated from

$$f_e = n_e \cdot \frac{4}{3}\pi\left(\frac{d^e}{2}\right)^3. \tag{3}$$

The growth surface area concentration, $S_{env,M}^e$, of the equivalent spheres is

$$S_{env,M}^e = \Phi_{Imp}^e \cdot (36\pi \cdot n_e)^{\frac{1}{3}} \cdot f_e^{\frac{2}{3}}, \tag{4}$$

where Φ_{Imp}^e is an impingement factor, which is here approximated as f_ℓ.

3.1.2. Growth of equiaxed grains

For the globular growth the morphology of the grain is simplified as a sphere and solute partitioning occurs at the liquid–solid interface, which is identical to the grain envelope. The growth of the grain is governed by diffusion around the growing sphere, and its growth velocity, v_{glob}^e, can be modelled analytically.

$$v_{glob}^e = \frac{D_\ell}{R^e} \cdot \Omega, \tag{5}$$

where Ω is supersaturation $(c_\ell^* - c_\ell)/(c_\ell^* - c_s^*)$.

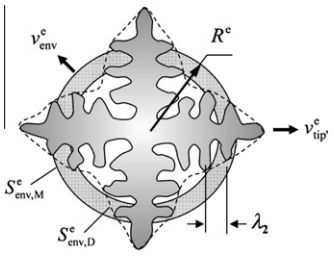

Fig. 2. The shape of the equiaxed dendritic grain envelope is simplified as a sphere that has a volume equivalent to the grain envelope (dashed line) connecting the primary and secondary dendrite tips.

Table 1
Morphological shape factors for envelopes of selected dendritic structures.

Equiaxed[a]		Columnar (cross section)	
Sphere $\Phi^{e}_{env}=1;\Phi^{e}_{sph}=1$		Cylinder $\Phi^{c}_{env}=1;\Phi^{c}_{circ}=1$	
Octahedral $\Phi^{e}_{env}=1/\sqrt[3]{\pi};\Phi^{e}_{sph}=\sqrt[3]{\pi}/\sqrt{3}$		Square rod $\Phi^{c}_{env}=\sqrt{2}/\sqrt{\pi};\Phi^{c}_{circ}=\sqrt{\pi}/2$	
OSP6[b] $\Phi^{e}_{env}=\sqrt[3]{11/32\pi};\Phi^{e}_{sph}=\frac{\sqrt[3]{484\pi}}{12+\sqrt{3}}$		OSW4[c] $\Phi^{c}_{env}=1/\sqrt{\pi};\Phi^{c}_{circ}=\sqrt{\pi/10}$	

[a] Equiaxed images taken from [28].
[b] 6 Orthogonal square pyramids (OSP6) [27] with pyramid angle 18.43°.
[c] 4 Orthogonal square wedges (OSW4) with wedge angle 60°.

For the dendritic growth, the growth velocity of the primary dendrite tips can be determined according to the LGK model [24,25].

$$v^{e}_{tip'}=\frac{D_\ell\cdot m_\ell\cdot c^{*}_\ell\cdot(k-1)}{\Gamma\cdot\pi^2}(Iv^{-1}(\Omega))^2. \tag{6}$$

Solving Eqs. (1) and (6) the growth velocity of the volume-equivalent sphere of dendritic grain, $v^{e}_{env,M}$, is obtained. The globular-to-dendritic transition (GDT) is determined by comparing the two growth velocities: v^{e}_{glob} and $v^{e}_{env,M}$. Therefore, the general formulation for the growth velocity of the equiaxed grain is

$$v^{e}_{env}=\max(v^{e}_{glob},v^{e}_{env,M}) \tag{7}$$

A straightforward approach is used to determine the globular-to-dendritic transition (GDT) by making a direct comparison of two growth velocities, v^{e}_{glob} and $v^{e}_{env,M}$. The validity of this approach was previously discussed [22,23]. It was verified that the grains start to grow with globular morphology at the initial stage. Once $v^{e}_{env,M}$ surpasses v^{e}_{glob}, GDT occurs and "free" dendritic growth commences. With the above v^{e}_{env} and $S^{e}_{env,M}$, the volume-averaged mass transfer rate $M_{\ell e}$ from ℓ-phase to e-phase can be calculated.

3.2. Columnar growth

3.2.1. Columnar morphology

A columnar trunk may grow with cellular or dendritic morphology. The cellular morphology can be simplified as a step-wise cylinder. The diffusion-governed growth of a cylinder is detailed elsewhere [19–21]. After cellular-to-dendritic transition (CDT), the morphology of the trunk becomes dendritic. To model the columnar dendritic growth, two zones must be considered: the zone containing only columnar trunks, and the zone containing columnar primary dendrite tips. In Fig. 3 the dendrite trunk is drawn within a fictitious grain envelope. Near the primary dendrite tip, the envelope borders the tips of primary and secondary dendrite, while in the zone far away from the primary dendrite tip the envelope borders the tips of secondary and tertiary dendrites. The longitudinal section of the envelope near the primary dendrite tip is similar to a paraboloid. The cross section of the dendrite trunk away from the primary dendrite tip can be described by a cylinder, square rod or four orthogonal square wedges connecting the secondary and tertiary dendrite tips (Table 1).

As in the equiaxed case, the complex geometry of the columnar trunk envelope necessitates a geometrical simplification of the envelope, in this case into a step-wise cylinder. The cross sectional area of the cylinder is equivalent to the area enclosed by the grain envelope. The term 'stepwise' indicates that the dendrite trunks, simplified as cylinders in a volume element, have an averaged diameter different from that in the neighbour volume element. The radial growth velocity of the equivalent cylinder can be calculated from the growth velocity of the secondary dendrite tip $v^{c}_{tip''}$,

$$v^{c}_{env,M}=\Phi^{c}_{env}\cdot v^{c}_{tip''} \tag{8}$$

where Φ^{c}_{env} is a shape factor. The diffusion area of the columnar envelope ($S^{c}_{env,D}$) is estimated according to the surface area of the equivalent cylinder ($S^{c}_{env,M}$) by considering a circularity factor Φ^{c}_{circ},

$$S^{c}_{env,D}=S^{c}_{env,M}/\Phi^{c}_{circ} \tag{9}$$

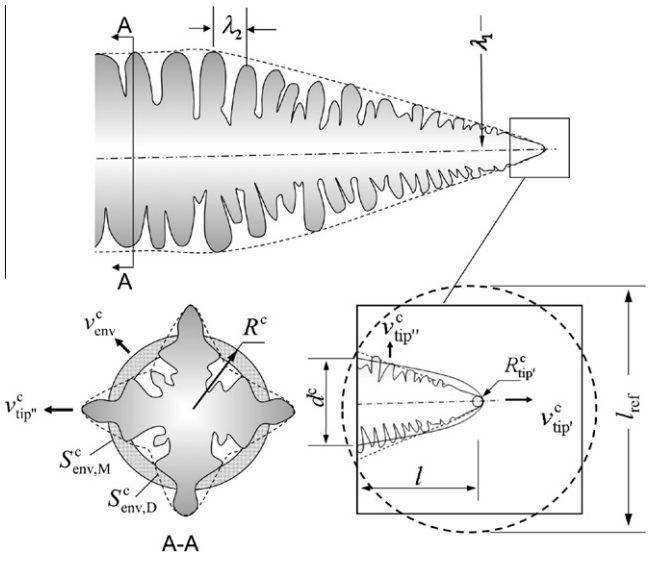

Fig. 3. The shape of the columnar trunk envelope is simplified as a step-wise cylinder with cross sectional area equivalent to the tree-trunk envelope (dashed line), which connects the secondary and tertiary dendrite tips. The contour of the columnar envelope near the primary dendrite tip (dashed line connecting the primary and secondary dendrite tips) is simplified as a paraboloid.

Examples of some columnar trunk envelopes (cross section) and their morphological shape factors are collected in Table 1. The accuracy and sensitivity of these shape factors will be addressed with model parameter studies. For solidification of cellular trunk, both Φ^{c}_{env} and Φ^{c}_{circ} are equal to one.

Given a constant primary dendrite arm spacing λ_1, the volume-equivalent cylinder has an average diameter of d^{c} (=$2R^{c}$), and they are correlated to the fraction of columnar phase by

$$f_c = \pi(d^{c}/2)^2/\lambda_1^2. \tag{10}$$

The surface concentration $S^{c}_{env,M}$ of the volume-equivalent cylinder is calculated with

$$S^{c}_{env,M} = \Phi^{c}_{Imp} \cdot \frac{\pi d^{c}}{\lambda_1^2}, \tag{11}$$

where Φ^{c}_{Imp} is an impingement factor, which is approximated as f_ℓ. Eqs. (10) and (11) apply for both cellular growth and dendritic growth. Eq. (11) is based on the assumption that the array of the columnar dendrite trunks is aligned. For the staggered array of the columnar dendrite trunks, the $\pi d^{c}/\lambda_1^2$ is replaced by $(2/\sqrt{3}) \cdot \pi d^{c}/\lambda_1^2$ [21].

Special consideration is made for the zone containing primary dendrite tips. A fictitious grain envelope (dashed line) enclosing the primary and secondary dendrite tips is shown in Fig. 3. This envelope is further simplified as a volume-equivalent paraboloid, described in Appendix A (Fig. A-2). In a volume element that contains primary dendrite tips, a paraboloid with a diameter of d^{c} and a length of l is used to represent the contour of the primary dendrite tip. The length of the paraboloid is explicitly tracked with a method that is described in Section 3.4. Within the volume-equivalent paraboloid two phases exist, i.e. solid dendrite and interdendritic melt. The same shape factor Φ^{c}_{env} and circularity Φ^{c}_{circ} are employed to simplify the shape of the parabolic envelope. The diameter d^{c} and surface concentration $S^{c}_{env,M}$ of the volume-equivalent paraboloid in the volume element containing primary dendrite tips are calculated as

$$f_c = \frac{\pi d^{c^2}}{8} \cdot l \cdot n_c, \tag{12}$$

$$S^{c}_{env,M} = \Phi^{c}_{Imp} \cdot S_{parab} \cdot n_c, \tag{13}$$

where S_{parab} is surface area of the paraboloid and n_c is "number density" of the columnar dendrites in the volume element containing primary dendrite tips, see Appendix A. Note that these expressions differ from Eqs. (10) and (11) for columnar trunk growth.

3.2.2. Growth of columnar dendrites

In the case of cellular, non-dendritic growth, the trunk is simplified to a cylinder and the radial growth velocity, v^{c}_{cell}, is governed by diffusion around the cylinder,

$$v^{c}_{cell} = \frac{D_\ell}{R^{c}} \cdot \Omega \cdot \ln^{-1}\left(\frac{\lambda_1}{\sqrt{3}R^{c}}\right) \tag{14}$$

A staggered array of the cellular trunks is assumed. The diameter of the cellular trunk is $2R^{c}$, with a maximum diameter of $2\lambda_1/\sqrt{3}$.

For the dendritic growth, the growth velocity of the secondary dendrite tip is determined by the LGK model [24,25], i.e. $v^{c}_{tip''} = v^{e}_{tip'}$. With Eq. (8) the growth velocity of the volume-equivalent cylinder, $v^{c}_{env,M}$, is obtained. The cellular-to-dendritic transition (CDT) is determined by comparison of the two growth velocities, thus, the general formulation for the growth velocity of the columnar trunk is:

$$v^{c}_{env} = \max(v^{c}_{cell}, v^{c}_{env,M}) \tag{15}$$

Similar to the approach used for determining GDT of equiaxed growth, the CDT is determined by making a direct comparison of two growth velocities, v^{c}_{cell} and $v^{c}_{env,M}$. With the above v^{c}_{env} and $S^{c}_{env,M}$, the volume-averaged mass transfer rate, $M_{\ell c}$, from ℓ-phase to c-phase can be calculated. Note that special consideration must be made for the volume element containing columnar dendrite tips. Additional contribution of the growth of the primary dendrite tips ($v^{c}_{tip'} \cdot \pi {R^{c}_{tip'}}^2$) to the total volume-averaged mass transfer within a volume element must be taken into account as well. The tip radius $R^{c}_{tip'}$ is calculated according to Kurz and Fisher [25], and the primary dendrite tip growth velocity, $v^{c}_{tip'}$, according to the Kurz–Giovanola–Trivedi (KGT) model [29],

$$v^{c}_{tip'} = k_1 \cdot \Delta T^2 + k_2 \cdot \Delta T^3 \tag{16}$$

where k_1 and k_2 are empirical growth parameters [30], and ΔT is undercooling.

3.3. Solidification of interdendritic melt

In both equiaxed and columnar growth, solidification of the interdendritic melt is driven by supersaturation and governed by diffusion in the interdendritic melt. The following model description applies to both equiaxed and columnar growth and is discussed in terms of equiaxed solidification (Fig. 4). The solidification rate of interdendritic melt is determined by d/s interface growth velocity v^{e}_{sd} and d/s interface area concentration S^{e}_{s}. The driving force for v^{e}_{sd} is $c^{*}_{\ell} - c^{e}_{d}$, but it is governed by diffusion at the length scale l^{e}_{d}, which is related to the secondary arm spacing λ_2 [2,22] by

$$l^{e}_{d} = \beta_2 \cdot \frac{(\lambda_2 - d_2)}{2}, \tag{17}$$

where β_2 is a constant on the order of unity and d_2 is the diameter of the secondary dendrite arms. It is assumed that d_2 is correlated to λ_2 by $\lambda_2 - d_2 = \lambda_2 \cdot \alpha^{e}_{d}$, thus

$$v^{e}_{sd} = \frac{2 \cdot D_\ell}{\beta_2 \cdot \lambda_2 \cdot \alpha^{e}_{d}} \cdot \frac{c^{*}_{\ell} - c^{e}_{d}}{c^{*}_{\ell} - c^{*}_{s}}. \tag{18}$$

The d/s interface area in an enclosed grain envelope is also related to the secondary arm spacing ($\propto 2/\lambda_2$). Considering an impingement factor $\Phi^{s}_{Imp} (= \alpha^{e}_{d})$ for the growing interfacial surface, the d/s interfacial surface concentration, in reference to the total volume, can be calculated as

$$S^{e}_{s} = \frac{2 \cdot \Phi^{s}_{Imp}}{\lambda_2} \cdot f_e. \tag{19}$$

For globular growth, the above equation does not apply, S^{e}_{s} must be equal to $S^{e}_{env,M}$ as calculated by Eq. (4).

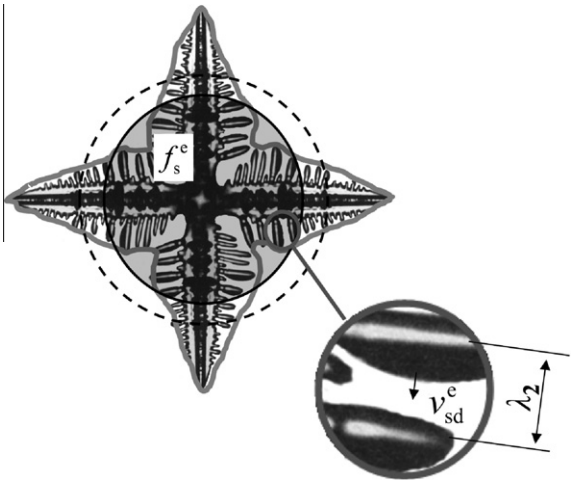

Fig. 4. Schematic of the interdendritic melt solidification.

3.4. Columnar tip tracking

The columnar trunks are assumed to grow from the mould wall. The chill zone, a layer of fine equiaxed crystals formed near the mould wall upon initial liquid contact, and the equiaxed-to-columnar transition (ECT) are ignored. The columnar primary dendrite tip front advances with the tip velocity $v^{c}_{tip'}$. No specific growth-preferred crystalline orientation is imposed. The columnar tip front is assumed to advance in the preferred direction that is closest to the temperature gradient due to the fact that the global solidification sequence is governed by the heat extraction of the mould. The position of the columnar tip front is explicitly tracked. The algorithm to track the columnar tip front is described below and shown schematically in Fig. 5. In this schematic example, the calculation domain is meshed with triangular elements. The following columnar tip front tracking algorithm applies to both structured and unstructured meshes, in both 2D and 3D.

(1) Each control volume element is indexed with a columnar status, i_c, which indicates whether the control volume element contains the columnar tips ($i_c = 1$), or the control volume has been passed by the columnar tips ($i_c = 2$), or the control volume is still in the bulk region where columnar tips do not yet reach ($i_c = 0$). All control volume elements are initialized with $i_c = 0$, except for the boundary (wall) elements, which are initialized with $i_c = 1$. The status marker with $i_c = 1$ indicates that the columnar trunks will start from these boundary elements.
(2) A reference length, l_{ref}, is assigned to each volume element to represent the element size. When a columnar tip enters a volume element, it must grow over the length of l_{ref} to be able to pass through the considered volume element. l_{ref} is calculated as the diameter of a sphere (3D) which has the equivalent volume of the element: $\frac{4\pi}{3}\cdot(l_{ref}/2)^3 = \Delta V$ (Appendix A). In case of 2D, l_{ref} is calculated as the diameter of an area-equivalent circle: $\pi\cdot(l_{ref}/2)^2 = \Delta S$. One may argue that depending on mesh topology and growth direction of the columnar tips, alternative methods should be used to determine l_{ref}, however, parameter studies have shown that alternative methods for estimating l_{ref} have a minor influence on modelling results [21].
(3) The columnar tip front is assumed to grow in the direction closest to the temperature gradient. The growth velocity, $v^{c}_{tip'}$, is determined by the KGT model [29]. The length of the columnar trunks belonging to the tip volume element ($i_c = 1$) is calculated by the integral $l = \int_t v^{c}_{tip'} dt$, starting from the moment when the columnar tip front enters the considered volume element.
(4) As soon as l exceeds l_{ref}, the columnar tip front grows out of the considered volume element and into the neighbouring control volume element, indexed with $i_c = 0$. The columnar status of the neighbouring element is converted into $i_c = 1$ and the status of the first volume element, which has just been passed by the columnar front, is set to $i_c = 2$.
(5) Mass transfer from the extradendritic melt (ℓ-phase) to the columnar trunk (c-phase) is only taken into consideration for those elements where $i_c \neq 0$. Mass transfer from the extradendritic melt (ℓ-phase) to the equiaxed grain (e-phase) can occur in all types of volume elements when a certain undercooling for nucleation and growth occurs.
(6) For the mechanical interaction between the e-phase and c-phase a simple approach is used. Both c- and e-phases are allowed to co-exist in the same volume element, even behind the columnar tip front. When the local volume fraction of c-phase, f_c, reaches a critical value, f_c^{free} (e.g. 0.2), an infinite drag force coefficient is applied between the phases in the corresponding momentum equations, and in effect the equiaxed grains are 'captured' by the columnar trunks. When f_c is smaller than f_c^{free}, no drag force is applied between e- and c-phases, and thus the motion of the equiaxed grains are free to move, unhindered by the columnar dendrites. The validation of the critical value $f_c^{free} = 0.2$ was discussed in a previous paper [21].
(7) The columnar tip blocking mechanism described by Hunt [31] is implemented to model the CET. In the columnar tip elements, the tip growth velocity, $v^{c}_{tip'}$, is forced to zero as soon as the local volume fraction of e-phase, f_e, exceeds the critical threshold of $f_{e,CET} = 0.49$. The so-called soft blocking mechanism for establishing the CET, proposed by Martorano et al. [11], is included, which reduces $v^{c}_{tip'}$ to zero when the local supersaturation vanishes due to the enhanced solute enrichment by the growing equiaxed grains ahead of the columnar dendrite tip front.

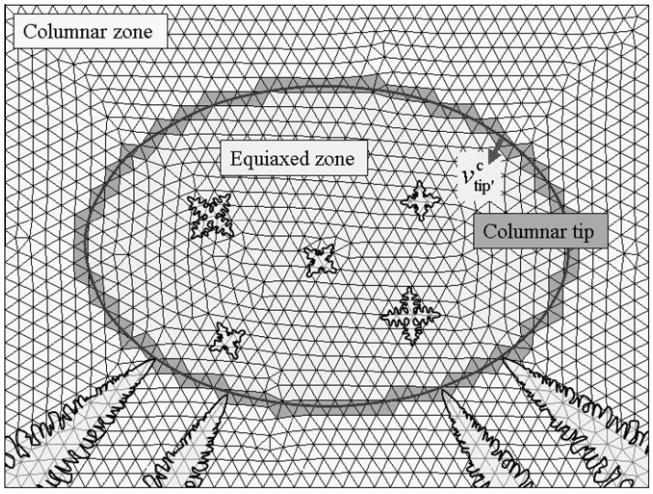

Fig. 5. Schematic diagram of the advancing columnar tip front, and the algorithm of the columnar front tracking during mixed columnar-equiaxed solidification. The equiaxed and columnar dendrites are shown to illustrate the two zones, they are not to scale relative to the grid.

4. Implementation of growth kinetics into transport equations

4.1. Transport equations

Sixteen independent transport quantities, n_e, f_e, f_c, f_s^e, f_s^c, p, $\vec{u}_\ell$, $\vec{u}_e$, c_ℓ, c_e, c_c, c_s^e, c_s^c, h_ℓ, h_e, h_c, are computed through solution of the conservation equations described below. Note that a velocity vector, e.g. $\vec{u}_\ell$, is here counted as a single transport quantity, although its components (u_ℓ, v_ℓ, w_ℓ) are necessarily solved by individual momentum conservation equation. Other intermediate variables can be derived from the above transport quantities. For example,

$$
\begin{aligned}
&f_\ell + f_e + f_c = 1 && \Rightarrow f_\ell = 1 - f_e - f_c,\\
&f_s^e = \alpha_s^e \cdot f_e && \Rightarrow \alpha_s^e = f_s^e/f_e, \alpha_d^e = 1 - \alpha_s^e, f_d^e = \alpha_d^e \cdot f_e,\\
&f_s^c = \alpha_s^c \cdot f_c && \Rightarrow \alpha_s^c = f_s^c/f_c, \alpha_d^c = 1 - \alpha_s^c, f_d^c = \alpha_d^c \cdot f_c,\\
&c_e = \alpha_d^e \cdot c_d^e + \alpha_s^e \cdot c_s^e \Rightarrow c_d^e = (c_e - \alpha_s^e \cdot c_s^e)/\alpha_d^e,\\
&c_c = \alpha_d^c \cdot c_d^c + \alpha_s^c \cdot c_s^c \Rightarrow c_d^c = (c_c - \alpha_s^c \cdot c_s^c)/\alpha_d^c.
\end{aligned}
$$

Temperatures, T_ℓ, T_e, T_c, are derived directly from the enthalpies, h_ℓ, h_e, h_c. All hydrodynamic phases share a single pressure field p. The pressure correction equation is obtained from the sum of the normalized mass conservation equations using the phase coupled

SIMPLE (PC-SIMPLE) algorithm [32]. The velocity of the columnar phase $\vec{u}_c$ is predefined.

The above transport quantities are solved using an Eulerian–Eulerian approach based on the three hydrodynamic phases. The formulations of the conservation equations for the three hydrodynamic phases are quite similar to those used in a previous three-phase mixed columnar-equiaxed (non-dendritic) solidification model [20]. Therefore, only the mass conservation and species conservation equations are described in detail.

The current model does not consider change of density due to thermo-solute expansion/shrinkage and solidification shrinkage. Although each phase density is indexed with ρ_ℓ, ρ_c, ρ_e, ρ_d^c, ρ_s^c, ρ_d^e, ρ_s^e (reserved for future use), in the current model they are constant and equal and the following equalities apply: $\rho_c = \alpha_s^c\rho_s^c + \alpha_d^c\rho_d^c$, and $\rho_e = \alpha_s^e\rho_s^e + \alpha_d^e\rho_d^e$. In order to account the thermo-solutal convection and grain sedimentation the Boussinesq approximation is used [33].

The mass conservation equations are

$$\frac{\partial}{\partial t}(f_\ell\rho_\ell) + \nabla\cdot(f_\ell\rho_\ell\vec{u}_\ell) = -M_{\ell e} - M_{\ell c} \tag{20}$$

$$\frac{\partial}{\partial t}(f_e\rho_e) + \nabla\cdot(f_e\rho_e\vec{u}_e) = M_{\ell e} - M_{ec} \tag{21}$$

$$\frac{\partial}{\partial t}(f_c\rho_c) + \nabla\cdot(f_c\rho_c\vec{u}_c) = M_{\ell c} + M_{ec} \tag{22}$$

$$\frac{\partial}{\partial t}(f_s^e\rho_e) + \nabla\cdot(f_s^e\rho_e\vec{u}_e) = M_{ds}^e \tag{23}$$

$$\frac{\partial}{\partial t}(f_s^c\rho_c) + \nabla\cdot(f_s^c\rho_c\vec{u}_c) = M_{ds}^c \tag{24}$$

For the case of pure globular growth, $M_{ds}^e = M_{\ell e}$. Similarly, for the case of pure cellular growth, $M_{ds}^c = M_{\ell c}$. Neglecting crystal segmentation and attachment phenomena, the mass transfer rate between the columnar and equiaxed phases M_{ec} is equal to zero.

The species conservation equations are

$$\frac{\partial}{\partial t}(f_\ell\rho_\ell c_\ell) + \nabla\cdot(f_\ell\rho_\ell\vec{u}_\ell c_\ell) = -C_{\ell e} - C_{\ell c} \tag{25}$$

$$\frac{\partial}{\partial t}(f_e\rho_e c_e) + \nabla\cdot(f_e\rho_e\vec{u}_e c_e) = C_{\ell e} - C_{ec} \tag{26}$$

$$\frac{\partial}{\partial t}(f_c\rho_c c_c) + \nabla\cdot(f_c\rho_c\vec{u}_c c_c) = C_{\ell c} + C_{ec} \tag{27}$$

$$\frac{\partial}{\partial t}(f_s^e\rho_e c_s^e) + \nabla\cdot(f_s^e\rho_e\vec{u}_e c_s^e) = C_{ds}^e \tag{28}$$

$$\frac{\partial}{\partial t}(f_s^c\rho_c c_s^c) + \nabla\cdot(f_s^c\rho_c\vec{u}_c c_s^c) = C_{ds}^c \tag{29}$$

where $C_{ec} \equiv 0$, when crystal segmentation and attachment are neglected.

Table 2
Mass transfer rates for equiaxed solidification.

Mass transfer rate	For globular growth	For dendritic growth
$(\ell \Rightarrow e)M_{\ell e}$	$M_{\ell e} = v_{env}^e \cdot S_{env,M}^e \cdot \rho_e$	(30)
$(d \Rightarrow s)M_{ds}^e$	$M_{ds}^e = M_{\ell e}$	$M_{ds}^e = v_{sd}^e \cdot S_s^e \cdot \rho_e$ (31)

4.2. Source terms

In order to close the above conservation equations, the corresponding source terms, $M_{\ell e}, M_{\ell c}, M_{ds}^e, M_{ds}^c, C_{\ell e}, C_{\ell c}, C_{ds}^e$, and C_{ds}^c, must be defined according to the aforementioned growth kinetics.

4.2.1. Mass and species transfer for equiaxed solidification

The volume-averaged mass and species transfer rates for equiaxed solidification are summarized in Tables 2 and 3 for globular growth and dendritic growth. For dendritic growth [22], species transfer between the extradendritic melt and the equiaxed grain $C_{\ell e}$ includes transport into the grain envelope due to the growth of the envelope, $C_{\ell e}^M$, and transport due to the diffusive flux from the interdendritic melt to the extradendritic melt, $C_{\ell e}^D$. Melting (shrinking of the grain envelope) is not considered in the current model.

4.2.2. Mass and species transfer for columnar solidification

The volume-averaged mass and species transfer rates for columnar solidification are summarized in Tables 4 and 5 for cellular growth and dendritic growth. For dendritic growth [22], the species transfer between the extradendritic melt and the columnar dendrite trunks $C_{\ell c}$ includes species transport into the dendrite trunk envelope due to growth of the envelope, $C_{\ell c}^M$, and species transport due to the diffusive flux from the interdendritic melt to the extradendritic melt, $C_{\ell c}^D$. Melting (shrinking of the tree-trunk envelope) is not considered in the current model.

In Tables 4 and 5, the contribution to the mass transfer rate due to growth of the columnar dendrite tips, $M_{tip'}^c$, is calculated as

$$M_{tip'}^c = n_c \cdot \pi (R_{tip'}^c)^2 \cdot v_{tip'}^c \cdot \rho_c \cdot f_\ell. \tag{47}$$

As shown in Tables 3 and 5, the diffusion length around the grain/trunk envelope l_ℓ (l_ℓ^e or l_ℓ^c) is determined by the growth velocity of the envelope, D_ℓ/v_{env}, where v_{env} represents v_{env}^e or v_{env}^c. A variety of alternative methods for estimating l_ℓ have been suggested, varying in complexity and ease of implementation [2,5,6,11,26,27]. In the present model the D_ℓ/v_{env} formulation is preferred for its reasonable approximation and numerical simplicity, as discussed in a previous publication [22]. The physical bounds of diffusion length l_ℓ dictate that it should never be larger than half of the inter-grain spacing. Two extreme cases where $l_\ell = D_\ell/v_{env}$ may lead to overestimation or unrealistic values should be avoided: (1) infinitely small envelope growth velocity and (2) the late stage of solidification when growing grains/trunks impinge upon one another. Additionally, it is assumed that l_ℓ is not smaller than the diffusion length of the interdendritic melt, l_d^e or l_d^c, therefore, the following corrections to l_ℓ are made,

$$l_\ell = \begin{cases} y_1/2 & \text{when } D_\ell/v_{env} \leqslant y_1/2 \\ D_\ell/v_{env} & \\ y_2/2 & \text{when } D_\ell/v_{env} \geqslant y_2/2 \end{cases} \tag{48}$$

where y_1 is the interdendritic spacing, which can be estimated as $2l_d^e$ for equiaxed grain, $2l_d^c$ for columnar dendrite and y_2 is the inter-grain spacing, which can be estimated as $(\lambda_1 - d^c)$ for columnar growth zone and $(\sqrt[3]{6/\pi n_e} - d^e)$ for equiaxed growth zone. Note

Table 3
Species transfer rates for equiaxed solidification.

Species transfer rate		For globular growth	For dendritic growth	
$(\ell \Rightarrow e)\ C_{\ell e} = C_{\ell e}^M + C_{\ell e}^D$	$C_{\ell e}^M$	$C_{\ell e}^M = c_s^* \cdot M_{\ell e}$ (32)	$C_{\ell e}^M = \bar{c}_{env}^e \cdot M_{\ell e}$	(33)
	$C_{\ell e}^D$	–	$C_{\ell e}^D = -\rho_\ell \cdot S_{env,D}^e \cdot J_\ell^e$ with $J_\ell^e = D_\ell \cdot (\bar{c}_{env}^e - c_\ell)/l_\ell^e$	(34)
$(d \Rightarrow s)C_{ds}^e$			$C_{ds}^e = c_s^* \cdot M_{ds}^e$	(35)

Table 4
Mass transfer rates for columnar solidification.

Mass Transfer rate	For cellular growth			For dendritic growth		
	Trunk element	Tip element		Trunk element	Tip element	
		$l > R^{c}_{tip'}$	$l \leqslant R^{c}_{tip'}$		$l > R^{c}_{tip'}$	$l \leqslant R^{c}_{tip'}$
$(\ell \Rightarrow c)\ M_{\ell c}$	See Eq. (36)	See Eq. (37)	See Eq. (38)	$M_{\ell c} = \nu^{c}_{env} \cdot S^{c}_{env,M} \cdot \rho_c$ (36)	$M_{\ell c} = \nu^{c}_{env} \cdot S^{c}_{env,M} \cdot \rho_c + M^{c}_{tip'}$ (37)	$M_{\ell c} = M^{c}_{tip'}$ (38)
$(d \Rightarrow s)\ M^{c}_{ds}$		$M^{c}_{ds} = M_{\ell c}$		$M^{c}_{ds} = \nu^{c}_{sd} \cdot S^{c}_{s} \cdot \rho_c$ (39)	$M^{c}_{ds} = \nu^{c}_{sd} \cdot S^{c}_{s} \cdot \rho_c + M^{c}_{tip'}$ (40)	$M^{c}_{ds} = M_{\ell c}$

Table 5
Species transfer rates for columnar solidification.

Species transfer rate		For cellular growth	For dendritic growth		
			Trunk element	Tip element	
				$l > R^{c}_{tip'}$	$l \leqslant R^{c}_{tip'}$
$(\ell \Rightarrow c) C_{\ell c} = C^{M}_{\ell c} + C^{D}_{\ell c}$	$C^{M}_{\ell c}$	$C^{M}_{\ell c} = c^{*}_{s} \cdot M_{\ell c}$ (41)	$C^{M}_{\ell c} = \bar{c}^{c}_{env} \cdot M_{\ell c}$ (42)	$C^{M}_{\ell c} = \bar{c}^{c}_{env} \cdot \nu^{c}_{env} \cdot S^{c}_{env,M} \cdot \rho_c + c^{*}_{s} \cdot M^{c}_{tip'}$ (43)	See Eq. (41)
	$C^{D}_{\ell c}$	/	$C^{D}_{\ell c} = -\rho_\ell \cdot S^{c}_{env,D} \cdot J^{c}_{\ell}$ with $J^{c}_{\ell} = D_\ell \cdot (\bar{c}^{c}_{env} - c_\ell)/l^{c}_{\ell}$ (44)	$C^{D}_{\ell c} = -\rho_\ell \cdot S^{c}_{env,D} \cdot J^{c}_{\ell}$ (45)	/
$(d \Rightarrow s) C^{c}_{ds}$			$C^{c}_{ds} = c^{*}_{s} \cdot M^{c}_{ds}$		(46)

that the model presented in Tables 3 and 5 for species transfer is not suitable for melting, when the envelope shrinks.

4.2.3. End of solidification

The solidification process ends with eutectic reaction, when both interdendritic melt and the extradendritic melt are converted into eutectic phases when the local temperature reaches the eutectic point T_E. Here a simple model is suggested. If the remaining liquid (i.e. eutectic phase) is relatively small, the latent heat released due to eutectic reaction is neglected and the aforementioned source terms ($M_{\ell e}, M_{\ell c}, M^{e}_{ds}, M^{c}_{ds}, C_{\ell e}, C_{\ell c}, C^{e}_{ds}, C^{c}_{ds}$) are set equal to zero as soon as the local temperature reaches T_E. Correspondingly, the drag forces that are applied between each pair of hydrodynamic phases are set 'infinitely' high [20], such that relative motion between the phases is prohibited. The remaining melt (both interdendritic and extradendritic) is recognized as eutectic phase, i.e. $f^{extra}_{Eu} = f_\ell, f^{intern}_{Eu,e} = f^{e}_{d}, f^{intern}_{Eu,c} = f^{c}_{d}$, and $f^{total}_{Eu} = f^{extra}_{Eu} + f^{intern}_{Eu,e} + f^{intern}_{Eu,c}$.

4.3. Solution strategy

A variety of computational tools for solving Eulerian multiphase transport system are available and discussed in the literature, each having distinct merits and drawbacks [34–37]. The model presented in the current paper is developed within the framework of the CFD software package, FLUENT 6.3.26 (Fluent Inc., USA) [32], which provides a platform for solving the global governing equations and provides flexibility in defining additional exchange and source terms within the governing equations, including modification of the transport quantities. For each time step of the transient calculation, up to 60 iterations may be necessary to decrease the normalized residuals of continuity, momentum conservation, volume fraction, species transport and user-defined scalar conservation equations to a value below the convergence limit of 10^{-4} and the enthalpy conservation equations below that of 10^{-7}. Due to the complexity of the multiphase coupling, the time step Δt should be kept small (10^{-3}–10^{-4}) to ensure the above convergent criteria are fulfilled. The optimal time step must be determined by trial simulations or by using dynamic time step control.

5. Summary and discussion

A five-phase volume-averaging solidification model has been proposed for the mixed columnar-equiaxed solidification with melt convection and grain sedimentation. The main difficulties encountered by the previous models have been addressed.

(1) Non-dendritic and dendritic solidification of the equiaxed and columnar structures are considered. For equiaxed structure, globular growth and dendritic growth including the globular-to-dendritic transition (GDT) are modelled. For columnar structure, cellular growth and dendritic growth including cellular-to-dendritic transition (CDT) are modelled. Both GDT and CDT are predicted based on comparison of growth velocities derived from diffusion-governed, non-dendritic growth kinetics and dendritic tip growth kinetics.
(2) Four morphological shape factors, $\Phi^{e}_{env}, \Phi^{e}_{sph}, \Phi^{c}_{env}$ and Φ^{c}_{circ}, are proposed to simplify the equiaxed and columnar dendritic structures. Previous studies on pure equiaxed solidification have justified the relevance of these factors [22,23]. However, these factors may not be constant and conserved during solidification, thus further studies are necessary to determine the accuracy of the morphological shape factors.
(3) An algorithm for columnar primary dendrite tip tracking is presented. This columnar tip front successfully distinguishes the pure equiaxed solidification zone from the mixed columnar-equiaxed zone. Two columnar primary dendrite tip blocking mechanisms, 'hard blocking' and 'soft blocking', are implemented for the prediction of the columnar-to-equiaxed transition (CET).
(4) The Boussinesq approximation is used to account for thermo-solutal convection and grain sedimentation including sedimentation-induced melt convection. It is currently assumed that the densities of all phases and phase regions are constant and equal. To account for shrinkage flow due to the density change of each individual phase (or phase region) further modification to the current model is required.

The ultimate goal of this model is to predict the as-cast macrostructure including the distinct equiaxed and mixed columnar-equiaxed zones separated by CET profile, the volume fraction of each phase or phase region, grain size, distribution of the eutectic phase, solute concentration in each phase or phase region, and macrosegregation. Due to the complex nature of the solidification process model assumptions or simplifications are necessarily made with the consequence of potential model uncertainties, which

must be clarified and resolved. To investigate these assumptions and simplifications illustrative process simulations, parameter studies and discussions are presented in Part II of this two-part investigation.

Appendix A

A.1. Geometric description of the columnar primary dendrite tip

A.1.1. Number density of columnar trunks in a volume element containing primary dendrite tips

The number density of columnar dendrite trunks in a volume element containing primary dendrite tips, n_c, is estimated. The columnar array is assumed to be aligned, and the primary dendrite arm spacing, λ_1, is constant. As shown in Fig. A-1 , a cubic volume element ($\Delta V = \Delta x^3$) contains $\Delta x^2/\lambda_1^2$ columnar dendrite trunks, therefore,

$$n_c = \frac{1}{\lambda_1^2 \cdot \Delta x}.$$

As the shape of each volume element is not consistent, a reference volume element length l_{ref} is used in place of Δx [21]. For a cubic element, $\frac{4\pi}{3} \cdot (l_{ref}/2)^3 = \Delta x^3$. So

$$n_c = \frac{1}{\lambda_1^2 \cdot l_{ref} \cdot \sqrt[3]{\pi/6}}. \quad \text{(A-1)}$$

A.1.2. Volume and surface area of paraboloid tip

A paraboloid is employed to simplify the shape of the envelope of the columnar primary dendrite tip. The geometry of a paraboloid (Fig. A-2) is expressed by

$$z = \frac{4l}{d^{c^2}} \cdot x^2. \quad \text{(A-2)}$$

The volume of the paraboloid, V_{parab}, is calculated by the integral $\int_0^l \pi x^2 dz$, with

$$V_{parab} = \frac{\pi d^{c^2}}{8} \cdot l. \quad \text{(A-3)}$$

The surface area of the paraboloid, S_{parab}, can be calculated by the integral $\int_0^l 2\pi x \cdot \frac{1}{\cos\theta} \cdot dz$, hence

$$S_{parab} = \frac{\pi d^c}{96 l^2} \cdot \left((16l^2 + d^{c^2})^{3/2} - d^{c^3} \right). \quad \text{(A-4)}$$

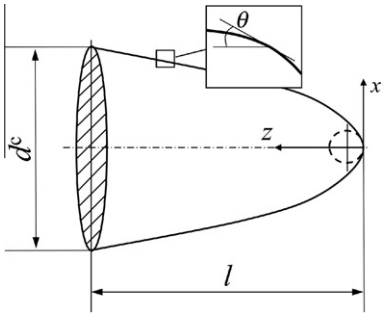

Fig. A-2. A simplified volume-equivalent paraboloid for the envelope of the columnar primary dendrite tip.

References

[1] C. Beckermann, R. Viskanta, Applied Mechanics Reviews 46 (1993) 1–27.
[2] C.Y. Wang, C. Beckermann, Metallurgical Transactions A – Physical Metallurgy and Materials Science 24 (1993) 2787–2802.
[3] C. Beckermann, C.Y. Wang, JOM – Journal of the Minerals Metals and Materials Society 46 (1994) 42–47.
[4] C.Y. Wang, C. Beckermann, Metallurgical and Materials Transactions A – Physical Metallurgy and Materials Science 27 (1996) 2754–2764.
[5] M. Rappaz, P.h. Thévoz, Acta Metallurgica 35 (1987) 1487–1497.
[6] M. Rappaz, P.h. Thévoz, Acta Metallurgica 35 (1987) 2929–2933.
[7] M. Rappaz, International Materials Reviews 34 (3) (1989) 93–123.
[8] B. Appolaire, Free growth of NH_4Cl equiaxed crystals settling in undercooled NH_4Cl–H_2O melts, PhD thesis, Institut National Polytechnique de Lorraine, France, 1999.
[9] Ø. Nielsen, B. Appolaire, H. Combeau, A. Mo, Metallurgical and Materials Transactions A – Physical Metallurgy and Materials Science 32 (2001) 2049–2060.
[10] C.Y. Wang, C. Beckermann, Metallurgical and Materials Transactions A – Physical Metallurgy and Materials Science 25 (1994) 1081–1093.
[11] M.A. Martorano, C. Beckermann, Ch-A. Gandin, Metallurgical and Materials Transactions A – Physical Metallurgy and Materials Science 34 (2003) 1657–1674.
[12] A.I. Ciobanas, Y. Fautrelle, Journal of Physics D: Applied Physics 40 (2007) 3733–3762.
[13] A.I. Ciobanas, Y. Fautrelle, Journal of Physics D: Applied Physics 40 (2007) 4310–4336.
[14] J. Ni, C. Beckermann, Metallurgical Transactions B – Process Metallurgy 22 (1991) 349–361.
[15] J. Ni, F.P. Incropera, International Journal of Heat and Mass Transfer 38 (1995) 1271–1284.
[16] J. Ni, F.P. Incropera, International Journal of Heat and Mass Transfer 38 (1995) 1285–1296.
[17] A. Ludwig, M. Wu, Metallurgical and Materials Transactions A – Physical Metallurgy and Materials Science 33 (2002) 3673–3683.
[18] M. Wu, A. Ludwig, A. Bührig-Polaczek, M. Fehlbier, P.R. Sahm, International Journal of Heat and Mass Transfer 46 (2003) 2819–2832.
[19] A. Ludwig, M. Wu, Materials Science and Engineering A – Structural Materials Properties Microstructure and Processing 413 (2005) 109–114.

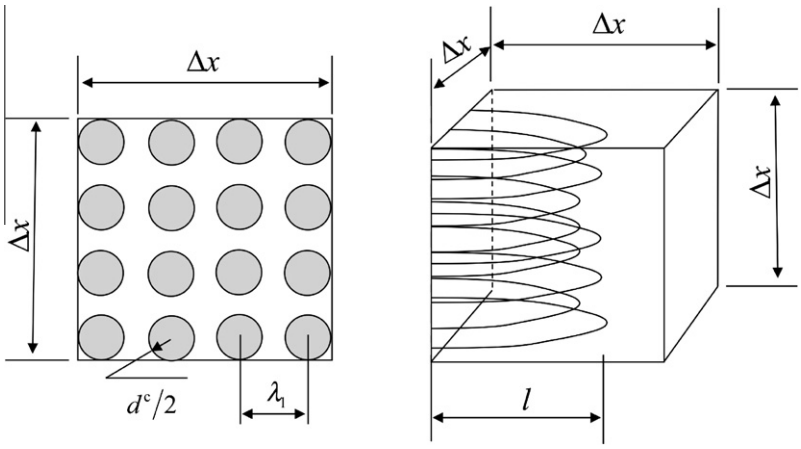

Fig. A-1. Aligned array of the columnar primary dendrite tips in a volume element.

[20] M. Wu, A. Ludwig, Metallurgical and Materials Transactions A – Physical Metallurgy and Materials Science 37 (2006) 1613–1631.
[21] M. Wu, A. Ludwig, Metallurgical and Materials Transactions A – Physical Metallurgy and Materials Science 38 (2007) 1465–1475.
[22] M. Wu, A. Ludwig, Acta Materialia 57 (2009) 5621–5631.
[23] M. Wu, A. Ludwig, Acta Materialia 57 (2009) 5632–5644.
[24] J. Lipton, M.E. Glicksman, W. Kurz, Materials Science Engineering 65 (1984) 57–63.
[25] W. Kurz, D.J. Fisher, Fundamentals of Solidification, fourth ed., Trans Tech, Zurich, 1998.
[26] A. Badillo, D. Ceynar, C. Beckermann, Journal of Crystal Growth 309 (2007) 197–215.
[27] A. Badillo, D. Ceynar, C. Beckermann, Journal of Crystal Growth 309 (2007) 216–224.
[28] T. Haxhimali, A. Karma, F. Gonzales, M. Rappaz, Nature Materials 5 (2006) 660–664.
[29] W. Kurz, B. Giovanola, R. Trivedi, Acta Metallurgica 34 (1986) 823–830.
[30] S.Y. Lee, S.M. Lee, C.P. Hong, ISIJ International 40 (2000) 40: 48–57.
[31] J.D. Hunt, Materials Science Engineering 65 (1984) 75–83.
[32] Fluent, Inc., Fluent 6.3 User's Guide, Fluent Inc., Lebanon, NH, USA, September 2006.
[33] D.D. Gray, A. Giorgini, International Journal of Heat and Mass Transfer 19 (1976) 545–551.
[34] N. Kolev, Multiphase Flow Dynamics I: Fundamentals, Springer Verlag, Berlin, 2002.
[35] N. Kolev, Multiphase Flow Dynamics II: Mechanical and Thermal Interactions, Springer Verlag, Berlin, 2002.
[36] C.E. Brennen, Fundamentals of Multiphase Flow, Cambridge University Press, Cambridge, 2005.
[37] S.V. Patankar, Numerical Heat Transfer and Fluid Flow, Hemisphere, New York, 1980.